A 2-D Random-Walk Mobility Model for Location-Management Studies in Wireless Networks

Kuo-Hsing Chiang and Nirmala Shenoy, *Associate Member, IEEE*

***Abstract*—In this work, a novel two-dimensional (2-D) random-walk mobility model is proposed, which can be used for studying and analyzing the location-area crossing rate and dwell time of mobile users in wireless networks. The development and application of the model under two cell structures, namely the square and hexagon cells, have been detailed. The analytical results obtained for location-update rates and dwell times have been validated using simulated and published results. The highlights of the model are its simplicity, minimal assumptions, and adaptability to conduct both "location-crossing rate" and "dwell-time" studies using the same model with slight modifications for either the square or hexagon cells. Using symmetry of mobile-user movement, a reduced number of computational states was achieved. A novel wrap-around feature of the model facilitates reduced assumptions on user mobility, which has also resulted in considerably reduced mathematical computation complexity. A regular Markov chain model was used for computing the average location-area crossing rate. A slightly modified model with absorbing states was used to derive the dwell time. This is the first model of its kind that can be used for studying area-crossing rates. To further emphasize the flexibility of the model, we have extended the model to study an overlapped location-area strategy. The study and analysis of overlapped locations areas has hitherto been difficult due to the complexity of the models.**

***Index Terms*—Land mobile radio cellular systems, Markov processes, modeling.**

I. Introduction

THE MOBILITY of users is a major advantage of wireless over fixed telecommunications systems. The signaling traffic and database processing to support the mobility of users are always key concerns in the design and performance of wireless networks. Mobility models play a key role in studying different mobility-management features such as registration, paging, handoff, and database approaches. A mobility model with minimum assumptions and that is simple to analyze will be very useful under such circumstances. In most wireless network performance studies, the cell is assumed to be either hexagon or square shaped [1], although in real life cell shapes may be highly irregular. Some authors assume a circular cell shape, especially those using a fluid flow model. However, in our work, we have restricted our analysis to hexagon and square cells; the model we propose can easily accommodate these two types of cell shapes.

In this work, we highlight a novel two-dimensional (2-D) random-walk model that can be used for studying and analyzing the location-area crossing rate and dwell time of mobile with slight modifications to the basic proposed model. The development and application of the model under two cell structures, namely the square and hexagon cells, have been detailed. In both cases, the analytical results obtained for location-update rates and dwell times have been validated using simulated and published results. The analytically obtained results from the model show excellent concurrence with simulated and published results. The highlights of the model are its simplicity, minimal assumptions, and adaptability to conduct both location-crossing rate and dwell-time studies using the same model with slight modifications for both square and hexagon cells. We have used mobile-movement symmetry within and across "location areas" and applied the "lumped-process" property of Markov chains to obtain a model with reduced computational states. A novel wrap-around feature has been used in these models to reduce constraints on mobile movements, thereby providing a more realistic roaming scenario. The model uses a set of aggregate states to trace user movement within one location area and then uses a set of special (asterisk) states when crossing the boundary of the location area. Due to the wrap-around technique, the movement of the mobile is modeled to enter the original states again from the special states, once the mobile starts moving within the new location area. The average number of location-area crossing rates or updates made by the user is obtained by solving for the regular Markov chain. A slightly modified model with absorbing states was used to derive the dwell time. This is the first model of its kind that can be used for studying area-crossing rates and dwell times using a simple model. To further emphasize the flexibility of the model, we extended it to study an overlapped location-area strategy. We have provided comparative results between the overlapped and nonoverlapped strategies. Overlap location-area strategies are commonly used concepts in cellular networks. However, the study and analysis of such overlapped configurations has been difficult, due to the requirement of complex models. We show that it is possible to study such overlapped location-area schemes by using the proposed model.

Location areas can be dynamic or static. The proposed model can be adapted to study location-area crossing rates and dwell time in both dynamic as well as static location-area strategies.

Manuscript received September 11, 2002; revised May 5, 2003, September 10, 2003, and October 28, 2003.

K.-H. Chiang is with the Royal Melbourne Institute of Technology (RMIT) University, Melbourne Victoria 3001, Australia (e-mail: Ian_Chiang@wneweb.com.tw).

N. Shenoy is with the Rochester Institute of Technology, Rochester, NY 14623 USA (e-mail: ns@it.rit.edu).

Digital Object Identifier 10.1109/TVT.2004.823544

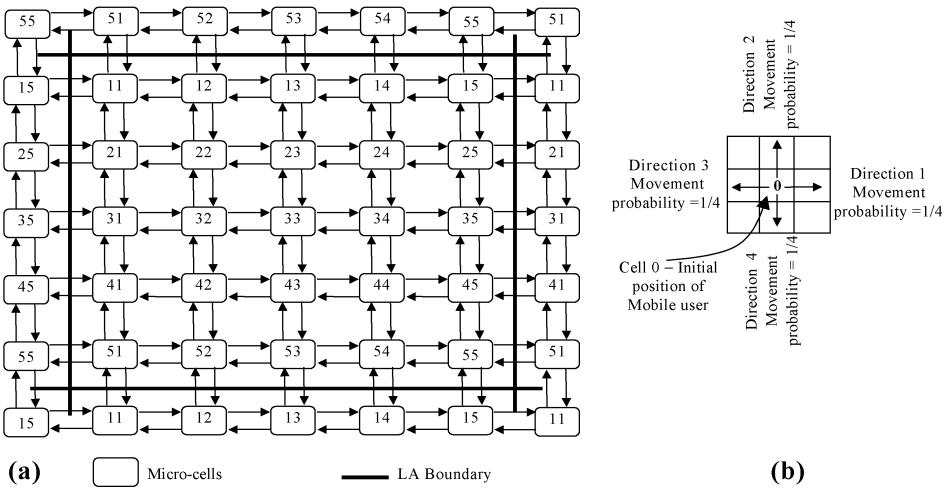

Fig. 1. Square-cell modeling approach.

The simple 2-D random-walk model is based on the properties of the regular and absorbing Markov chain. The regular model is used for computing the location-update rates. The same model with absorbing states is used to derive the dwell time in an area. There are far fewer computational states in the model, making its analysis easy. A "wrap-around" feature has been introduced in the model, which facilitates estimating location-update rate using simple equations. The model can be adapted to both square and hexagon-cell structures. Due to the simplicity of calculations, the model can be extended to study overlapped location-areas strategies, which has hitherto been difficult to handle. These are features that make the model ideally suited to mobility-management studies in cellular networks, although with the limitation that the cells will be either square or hexagon shaped.

Numerous works can be found in the literature that address mobility modeling and various models have been proposed by researchers to efficiently apply analytical and simulation models for mobility studies. Below, we highlight some of these models. At the end of this section, we highlight the features of our model that make it simple to use and adaptable to various mobility studies.

The fluid-flow model in [2]–[4] and [14] and the random-walk model are the two main types of mobility model that have been applied in location-management studies. The fluid-flow model can derive the average rate of boundary crossings per unit time out of a given area, but it is difficult to apply the model to the modern per-user-based location-area strategies or to study overlapped area-strategy performance. Most random-walk models are designed for dynamic location-area strategy [6], [7] or for deriving the dwell time [1], [5]. In [1], the authors have proposed a random-walk model that requires solving for complex mathematical equations, which we were able to avoid due to the wrap-around mechanism. In [11], the authors propose a novel approach to mobility modeling capturing the moving-in groups, conscious traveling, and inertial behavior of the subscribers in real life, using the locus of the mobile user in a terrain. In [12], a free-space propagation model using a global positioning system (GPS) is proposed by the authors, which is more suited to *ad hoc* networks. In [13], a three-level model is proposed, covering city-area, area-zone, and street-unit models.

Section II describes the development of the 2-D random-walk mobility model for both square and hexagon cell clusters. In Section III, the mathematical analysis for location update and dwell time for both cell structures are described. Section IV provides model validation by providing comparative results from the analytical model, a simulated model, and published results. Highlights of the model are given in Section V and in Section VI the overlapped location-area modeling is explained. Conclusions are given in Section VI.

II. 2-D Random-Walk Model

Users in cells belonging to a location area (LA) have identical movement pattern within and across LAs. Such cells can be assigned to a single state in the Markov chain using the lumped process property. This property has been applied here to achieve reduced computational states in the model. A state that lumps a number of cells with identical movement pattern is called an "aggregate state." In the next two sections, the derivation of the 2-D random-walk model for the square and hexagon cells is presented.

A. Model for Square Cells

Fig. 1(a) shows an LA configuration for $n*n$ square cells where $n = 5$. The bold lines indicate the boundary of the LA. Cells in the adjacent LAs are shown outside the thick boundary lines. There are 25 cells in the LA, which have been numbered, identifying each cell with its row and column position. It is assumed that the mobile user can move in four directions only, with an equal probability of 1/4 in each direction, as shown in Fig. 1(b). In Fig. 1(a), arrows show the possible user movement across cells within one LA and across LAs. In some of the cells, with reference to the LA, the mobile user will have identical movement patterns to other cells within the same LA and to cells in adjacent LAs. For example, from cells numbered 11, 15, 55, and 51, the mobile-user movement pattern and transition probabilities will be identical but rotated by 90°. The rotation of the movement pattern will not affect the studies to be

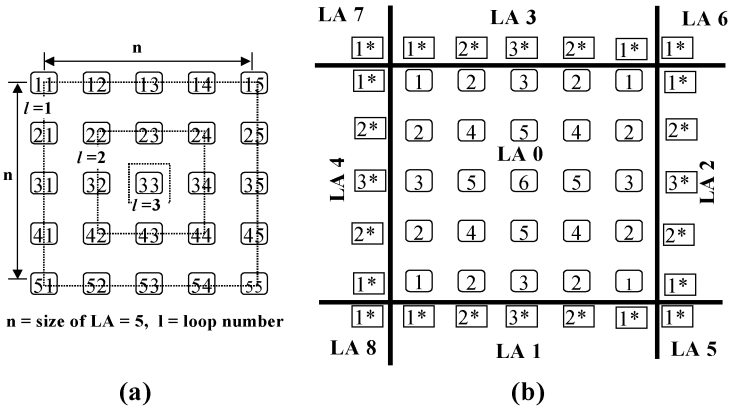

Fig. 2. State aggregation in the square-cell model.

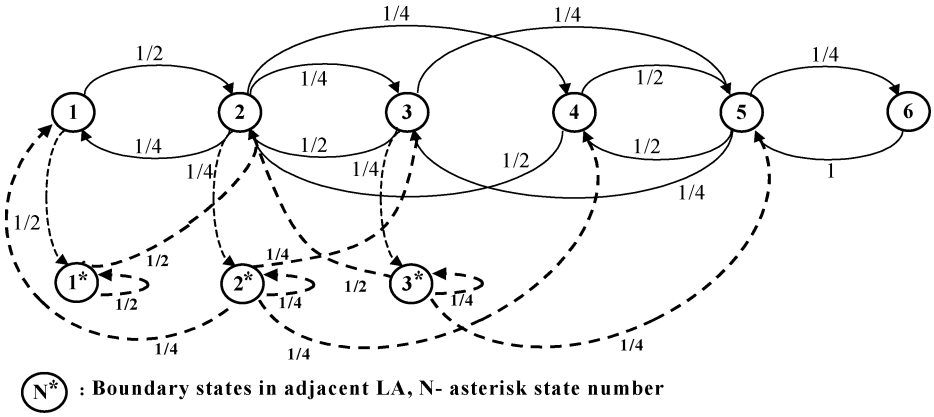

Fig. 3. State-transition diagram for 5×5 square-cell model.

conducted using Markov chains. Hence, these four cells can be grouped into one aggregate state in the Markov chain model. This property of lumping the states was carried out to reduce the total number of computational states in the mathematical analysis. An algorithm to perform state aggregation is given below [Figs. 2(a) and (b) are provided to explain the aggregation process].

1) Number the cells belonging to an LA as "rc," where r is the row number and c is the column number, as shown in Fig. 1(a). The numbering scheme has been applied to the cells in the adjacent LAs also, i.e., cells just outside the bold lines.
2) As shown as in Fig. 2(a), assign the cells to different loops. In this case, there are three loops. Let $l =$ number of loops. Then, $l = 1$ is the outer loop, $l = 2$ is the next loop, and $l = 3$ is the innermost loop. Cell 33 belongs to loop 3. Cells numbered 22, 23, 24, 34, 44, 43, 42, and 32 belong to loop 2. The rest of the cells in the LA belong to loop 1.
3) Let S_{rc} be the cell numbered "rc" and S_{cr} is the cell numbered "cr".

```
Start with n = 5, l = 1
  until (n = l).
  Repeat {x = l, y = n
    until (x > y).
    Repeat {set S_l^x = {S_rc ∪ S_cr}
      where r = l for c = x, y and
      r = n for c = x, y
      x = x + 1; y = y − 1;
    }
    n = n − 1, l = l + 1.
  }
```

Let $S_l{}^x$ be the aggregate state obtained as a set of the cells S_{rc} and S_{cr}.

After the aggregation process, the following state aggregation is obtained:

$$\begin{aligned}
&S^1{}_1 = \{S_{11}, S_{51}, S_{15}, S_{55}\},\\
&S^1{}_2 = \{S_{21}, S_{25}, S_{41}, S_{45}, S_{12}, S_{52}, S_{14}, S_{54}\},\\
&S^1{}_3 = \{S_{31}, S_{35}, S_{13}, S_{53}\}.\\
&S^2{}_1 = \{S_{22}, S_{24}, S_{42}, S_{44}\},\\
&S^2{}_2 = \{S_{32}, S_{34}, S_{23}, S_{43},\}.\\
&S^3{}_1 = \{S_{33}\}.
\end{aligned}$$

For ease of use, the aggregate states were assigned numbers, as follows:

$$S^1{}_1 \rightarrow 1,\ S^1{}_2 \rightarrow 2,\ S^1{}_3 \rightarrow 3,\ S^2{}_1 \rightarrow 4,\ S^2{}_2 \rightarrow 5\ S^3{}_1 \rightarrow 6.$$

We now have six aggregate states. The LA is redrawn in Fig. 2(b) with the cells numbered with their newly assigned aggregate state numbers. In Fig. 2(b), aggregate states 1, 2, and 3 are in the boundary of the LA and are called the "boundary" states. We further define "asterisk-boundary" states (or "star

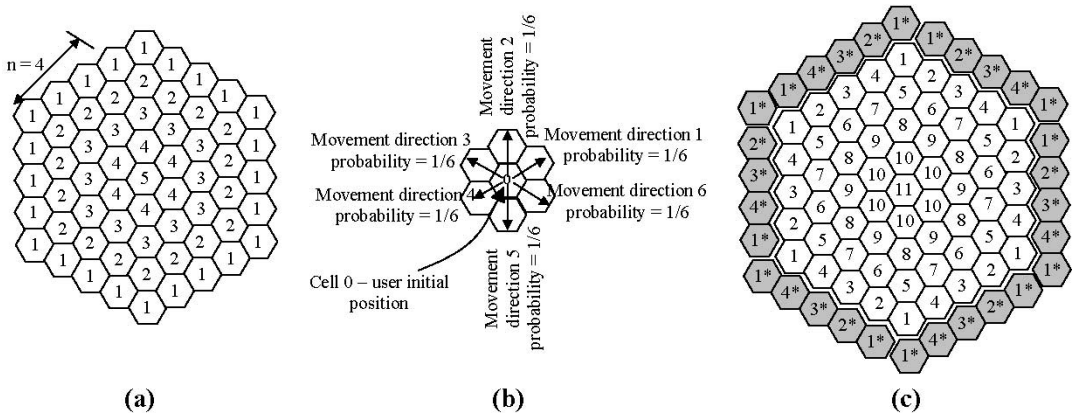

Fig. 4. State aggregation in the hexagon-cell model.

states"), i.e.,$1*$, $2*$ and $3*$, which are the boundary states in the adjacent LAs. Let LA0 be the LA under consideration in Fig. 2(b). LA1, LA2, LA3, and LA4 are the adjacent LAs. From LA0, a user can only move into any one of these adjacent LAs.

Using the direction and movement probabilities given in Fig. 1(b), the state-transition diagram for the regular Markov chain based on the aggregate states can be derived as shown in Fig. 3. In this approach, the entire movement of the mobile user across different cells and across LAs is modeled. The "asterisk-boundary" states and the wrap-round mechanisms, which will be explained shortly, achieve this freedom-of-movement feature. Movement into an "asterisk-boundary" state indicates a location-area crossing and can be used to study the location-area crossing rates or location updates.

A brief description of the operation of the state-transition diagram of Fig. 3 is now provided. As long as the user moves within cells in a location area, he is in one of the main aggregate states, i.e., 1, 2, 3, 4, 5, or 6. His movement is accordingly traced by the transitions shown and transition probabilities are marked beside the transition. The dotted transitions to the asterisk states indicate the mobile user's transition to a boundary state in an adjacent location area and the probabilities of such transitions are given beside these dotted transitions. These transitions accordingly model the mobile user's movement probability from the main location-area cells to the adjacent location-area cells. While in an asterisk state, the user can move across to other asterisk states. For example, in Fig. 2(b), the user can move from $1*$ in LA3 to $1*$ in LA7 or from $2*$ in the adjacent LA3 back to 2 in LA0 (2 in LA0 now would be $2*$ from the mobile user perspective as it is in an adjacent LA). In Fig. 3, this movement is modeled by the dotted transitions to itself in the asterisk states. Looking at the user movement from state $1*$ in LA3 [Fig. 2(b)], the user has a probability of 1/4 to move into state $1*$ in LA7 and probability of a 1/4 to move into state 1 in LA0 (which is now state $1*$ in the adjacent LA from the user perspective); hence, a transition probability of 1/2 to itself in state $1*$ is shown in Fig. 3.

When the user starts moving in the new LA, for example when he moves from state $1*$ in LA3 to $2*$ in LA3 or from $2*$ to $1*$ in LA3, the model wraps back to the normal states, indicating that the user has now started moving in cells belonging to the new LA. This is shown by the dotted transitions from the asterisk states to the normal states in Fig. 3. This novel wrap-around feature has subsequently led to the possibility of studying the location-area crossings by using simple equations.

This model can be applied at various levels of the network hierarchy. It can used to study the LA crossing and dwell time within one visitor location area (VLR) and the traffic due to VLR crossing at the next higher level in the hierarchy. The examples provided below illustrate the use of this model only for location-area crossing and area dwell time.

B. Model for Hexagon Cells

The model is now applied to hexagon cells. The cell- or state-aggregation process is slightly different and will be explained. Fig. 4(a) shows an LA of size $n = 4$ with hexagon cells. Each LA covers $1+\sum_1^n 6n$, i.e., 61 cells if $n = 4$. As seen in Fig. 4(b), the user movement is restricted to six directions with an equal probability of 1/6 in each direction. The following are the steps used for state aggregation.

1) Cells in the LA are assigned to loops and are numbered according to the loop to which they belong. With reference to Fig. 4(a), all cells belonging to loop 1 are numbered 1, those belonging to loop 2 are numbered 2, and so on. Let $l =$ number of loops. As can be seen, there are five loops, where loop 5 has only one cell.
2) Let $l = 1$. Let $c_{\max}$ be the starting cell number. Set $c_{\max} = 1$.
3) Starting from one corner of the hexagon, move in a clockwise direction and allocate cell numbers starting from $c_{\max} = 1$ in an increasing order till the next corner is reached. Stop numbering at the cell just before the next corner cell.
4) Repeat 3), starting from the next corner cell, until the outer loop is completed. The new cell numbers are shown in the unshaded cells in Fig. 4(c). The maximum cell number allocated is 4 in loop $l = 1$.
5) Set $c_{\max} =$ maximum cell number $+ 1$.
6) In loop $l = 2$, start at the corner cell and move clockwise and start numbering from $c_{\max}$ in increasing order until the next corner is reached. As before, stop at the cell just before the next corner.
7) Repeat from all corners in that loop, starting with the same $c_{\max}$ value, until all cells in the loop are numbered.
8) Repeat step 5, 6, and 7 for the rest of the loops.

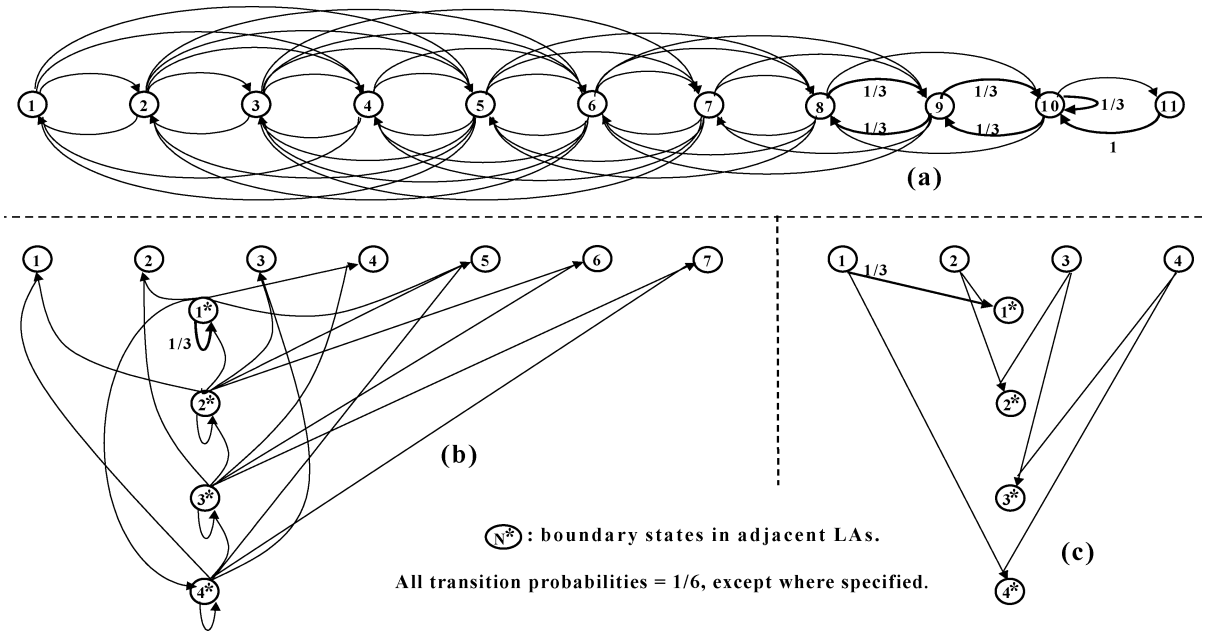

Fig. 5. State-transition diagram for the hexagon-cell model.

State aggregation has thus been completed. [The shaded cells in Fig. 4(c) are the cells in the adjacent LA.] From Fig. 4(c), aggregate state 1 = all cell marked 1, 2 = all cells marked 2, and so on. The states that aggregation obtained are similar to [1], but use a simple algorithm to perform the state aggregation.

As was done for the case of square cells, "asterisk-boundary" states are defined and identified in Fig. 4(c) for the hexagon cells. There are 11 aggregate states and four asterisk-boundary states in the Markov model. For clarity, the state-transition diagram has been provided in three parts. Fig. 5(a) is the transition diagram for states or cells within a locations area. Figs. 5(b) and (c) are for transitions across cells in the adjacent location areas. For the transition diagram, a similar explanation as used in the square-cell case can be extended and, hence, is not provided.

III. Model Analysis

It is assumed that each LA has similar properties and is of size n with $n*n$ square cells or $1+\sum_1^n 6n$ hexagon cells. The state-transition diagram for the Markov model for the user movement in LA, comprised of square cells, is shown in Fig. 3. The state-transition diagram for mobility in an LA that is comprised of hexagon cells is shown in Fig. 5. The general format for the transition probability matrix P in either case is given as

$$\mathbf{P}=[\mathrm{p_{ij}}]$$

$$\begin{array}{c} \\ 1* \\ 2* \\ \vdots \\ =N* \\ 1 \\ 2 \\ 3 \\ \vdots \end{array}\begin{array}{c} \begin{array}{cccccccc} 1* & 2* & \cdots & N* & 1 & 2 & 3 & \cdots \end{array} \\ \begin{pmatrix} \mathrm{p}_{11}^{**} & \mathrm{p}_{12}^{**} & \cdots & \mathrm{p}_{1N}^{**} & \mathrm{p}_{11}* & \mathrm{p}_{12}* & \mathrm{p}_{13}* & \cdots \\ \mathrm{p}_{21}^{**} & \mathrm{p}_{22}^{**} & \cdots & \mathrm{p}_{2N}^{**} & \mathrm{p}_{21}* & \mathrm{p}_{22}* & \mathrm{p}_{23}* & \cdots \\ & & \cdots & & & & & \\ \mathrm{p}_{N1}^{**} & \mathrm{p}_{N2}^{**} & \cdots & \mathrm{p}_{NN}^{**} & \mathrm{p}_{N1}* & \mathrm{p}_{N2}* & \mathrm{p}_{N3}* & \cdots \\ \mathrm{p}_{11}* & \mathrm{p}_{12}* & \cdots & \mathrm{p}_{1N}* & \mathrm{p}_{11} & \mathrm{p}_{12} & \mathrm{p}_{13} & \cdots \\ \mathrm{p}_{21}* & \mathrm{p}_{22}* & \cdots & \mathrm{p}_{2N}* & \mathrm{p}_{21} & \mathrm{p}_{22} & \mathrm{p}_{23} & \cdots \\ \mathrm{p}_{31}* & \mathrm{p}_{32}* & \cdots & \mathrm{p}_{3N}* & \mathrm{p}_{31} & \mathrm{p}_{32} & \mathrm{p}_{33} & \cdots \\ \cdots & & \cdots & & & & \cdots & \end{pmatrix} \end{array}.$$

$1*, 2*, \ldots, N*$ are the asterisk boundary states for that configuration.

In the following sections, a derivation of the LA update is first provided and then the dwell-time derivation is given. The section that follows briefly explains the simulation process.

A. Analysis for LA Updates

The state-transition diagrams in Figs. 3 and 5 show that there no transient sets in the model, but only a single ergodic set with only one cyclic class; hence, the regular Markov chain properties can be applied to analyze the behavior of the proposed model [10].

Let $\mathbf{P}$ be the regular transition probability matrix; then, the steady state (limiting) probability vector $\boldsymbol{\pi}$ can be solved by

$$\pi P = \pi \text{ and } \sum_{i=1}^{m} \pi_i = 1 \tag{1}$$

where m is the number of states.

$\mathbf{Z}$, the *fundamental matrix* for the regular Markov chain, is given by

$$\mathbf{Z} = [\mathrm{z}_{ij}] = (\mathbf{I} - \mathbf{P} + \mathbf{A})^{-1} \tag{2}$$

where

1) $\mathbf{A}$ is a limiting matrix determined by $\mathbf{P}$ and the powers $\mathbf{P}^n$ approach the probability matrix $\mathbf{A}$.
2) Each row of $\mathbf{A}$ comprises of the same probability vector $\pi = \{\pi_1, \pi_2, \ldots, \pi_n\}$, i.e., $\mathbf{A} = \xi\pi$, where ξ is column vector with all entries equal to 1.
3) $\mathbf{I}$ is the identity matrix.

Matrix $\mathbf{A}$ can be obtained by evaluating the power matrix of $\mathbf{P}$ and using high values of $\boldsymbol{n}$ so that the entries in each row converge.

The matrix $\mathbf{Z}$ can be used to study various behaviors of the regular Markov chain. Using this matrix, we compute the mean number of times the process is in a particular state [10].

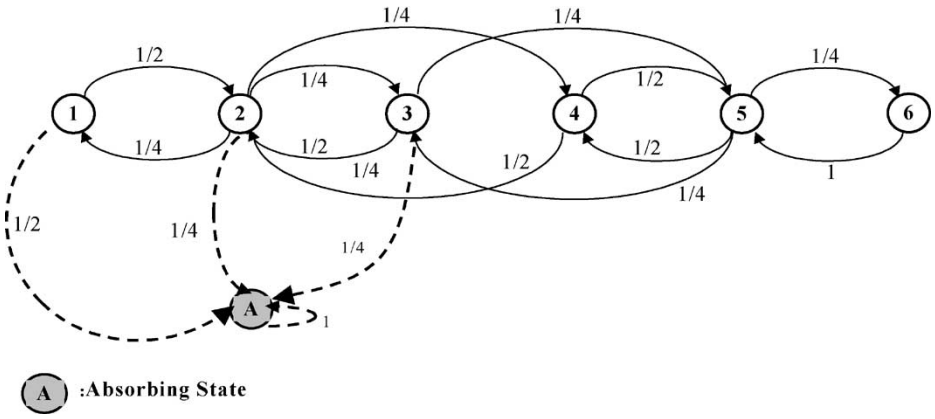

Fig. 6. Transition-state diagram for the square-cell model with absorbing state.

TABLE I
AVERAGE LOCATION-UPDATE RATES FOR THE SQUARE-CELL MODEL

S_i	1	2	3	4	5	6
U_{A_LU}	4.6	4	3.8	3.4	3.2	3
U_{S_LU}	4.5949	3.9958	3.7908	3.4078	3.2016	2.9969
RE %	0.12	0.11	0.24	0.23	0.05	0.10

S_i – Initial state of the user, RE – Relative Error

Let ${y_j}^{(k)}$ be the number of times that a process is in the state S_j in the first k steps. Then, $M_i[{y_j}^{(k)}]$, the mean number of times the process gets into state S_j starting from state S_i, is given by

$$M_i\left[{y_j}^{(k)}\right] \rightarrow (z_{ij} - \pi_j) + k\pi_j. \tag{3}$$

z_{ij} and π_j can be obtained from the matrices $\mathbf{Z}$ and $\mathbf{A}$ (or π), respectively.

The total number of boundary updates in k steps starting from state S_i can be computed by the total number of times that the process is in the asterisk states (for example, $1*$, $2*$, and $3*$ in Fig. 3) starting from state S_i, the initial state. Hence, if U_{A_LA} is the average number of location updates in the analytical model, this is given by

$$U_{A\_\mathrm{LA}} = M_i\left[{y_{1*}}^{(k)}\right] + M_i\left[{y_{2*}}^{(k)}\right] + M_i\left[{y_{3*}}^{(k)}\right] \tag{4}$$

where ${y_{1*}}^{(k)}$ is the the number of times that the process is in state $1*$, given that it started from some initial state and $M_i[{y_{1*}}^{(k)}]$ will give the mean number of times that the process in state $1*$, given that it started from an initial state S_i.

Generalizing,

$$U_{A\_\mathrm{LA}} = \sum_{n=1*}^{N*} M_i\left[y_n^{(k)}\right] \tag{5}$$

where $1*, 2*, \ldots, N*$ are the asterisk states in the model and S_i is the initial state.

B. Analysis for Dwell Time

To study the dwell time in a location area, the transition diagram of Figs. 3 and 5 are modified by converting the asterisk-boundary states into an absorbing state. The transition diagram of Fig. 3 is reproduced as Fig. 6 to demonstrate the modification of the regular model into an absorbing Markov chain.

According to the property of an absorbing state, once it is entered, it cannot be left. Hence, there is self-transition to this state with probability 1. By using the properties of the absorbing Markov chain, we can derive the LA dwell time (time to LA update), which is equal to the time to absorption. The transition matrix can generally be written in its canonical form. For an absorbing Markov chain, the canonical form is given by

$$\mathbf{P} = \left[\begin{array}{c|c} \mathbf{I} & \mathbf{0} \\ \hline \mathbf{R} & \mathbf{Q} \end{array}\right]. \tag{6}$$

where

- $\mathbf{I}$ is a square matrix of absorbing states. If there are n absorbing states, then the size of this matrix is $n*n$.
- $\mathbf{R}$ is a one-step transition probability from nonabsorbing state to absorbing states. If the number of nonabsorbing states is m, then the size of this matrix is given by $m*n$.
- $\mathbf{Q}$ is a square matrix giving the one-step transition probability from nonabsorbing state to nonabsorbing states. The size of this matrix is $m*m$.

Let $\mathbf{N}$ be the fundamental matrix for an absorbing Markov chain. Then, $\mathbf{N}$ is given by

$$\mathbf{N} = (\mathbf{I} - \mathbf{Q})^{-1}. \tag{7}$$

Let $\mathbf{t}$ be the function giving the number of steps (including the original position) in which the process is in a transient state. If the process starts in an ergodic state, the $\mathbf{t} = 0$. If the process starts in a transient state, then $\mathbf{t}$ gives the total number of steps needed to reach an ergodic state. In an absorbing chain, this is the time to absorption. From [5] and [10], the mean time to absorption from initial state S_i is given by

$$M_i[\mathbf{t}] = N\xi = U_{A\_D}. \tag{8}$$

This is the row sums of fundamental matrix $\mathbf{N}$, where ξ is the column vector with all entries equal to 1. U_{A_D} is the average dwell time for a user residing in initial state Si.

C. Simulation

Simulation of the user mobility was done using Monte Carlo methods. In each iteration of the simulation, a set of random numbers is generated. These random numbers are distributed

TABLE II
AVERAGE LOCATION-UPDATE RATES IN THE HEXAGON-CELL MODEL

S_i	1	2	3	4	5	6	7	8	9	10	11
U_{A_LU}	3.8830	3.5333	3.3552	3.4563	2.8943	2.6132	2.6022	2.1630	2.0163	1.7210	1.5734
U[illegible]	[illegible]	[illegible]	[illegible]	[illegible]	[illegible]	[illegible]	[illegible]	[illegible].1624	2.0146	1.7366	1.5876
RE	0.041	0.054	0.284	0.154	0.093	0.092	0.104	0.028	0.084	0.8981	0.894

S_i – Initial state of the user, RE – Relative Error%,

TABLE III
AVERAGE DWELL TIME IN THE SQUARE-CELL MODEL

S_i	1	2	3	4	5	6
U_{A_D}	3.8077	5.6154	6.1538	8.5	9.3846	10.385
U_{S_D}	3.8011	5.6091	6.5254	8.5036	9.3905	10.388
RE	0.174	0.112	0.008	0.042	0.063	0.028

S_i – Initial state of the user, RE – Relative Error %

uniformly on 1, 2, 3, and 4 for the square-cell model and on 1, 2, 3, 4, 5, and 6 for the hexagon-cell model. Based on the random number, the user moves to one of the adjacent cell from a starting cell 0.

Whenever the mobile user moves across the LA boundaries, the counter for location update is increased by one. If the total number of iterations is $M_E = 100\,000$, then the average number of location updates U_{S_LU} is calculated by

$$U_{S\_\mathrm{LU}} = \frac{1}{M_E}\sum_{x=1}^{M_E} M_i(x) \tag{9}$$

where x is the xth experiment and has the xth random number set and sequence.

IV. MODEL VALIDATION

A. Location-Update Rate in the Square-Cell Model

The number of computational states required for the 5 × 5 square shaped model is nine (six normal aggregate states and three asterisk states). The regular transition matrix for this model (derived from Fig. 3) is

$$\mathbf{P} = [\mathrm{p_{ij}}] = \begin{array}{c} \\ 1* \\ 2* \\ 3* \\ 1 \\ 2 \\ 3 \\ 4 \\ 5 \\ 6 \end{array}\!\!\begin{array}{c} \begin{array}{ccccccccc} 1* & 2* & 3* & 1 & 2 & 3 & 4 & 5 & 6 \end{array} \\ \left(\begin{array}{ccccccccc} \frac{1}{2} & 0 & 0 & 0 & \frac{1}{2} & 0 & 0 & 0 & 0 \\ 0 & \frac{1}{4} & 0 & \frac{1}{4} & 0 & \frac{1}{4} & \frac{1}{4} & 0 & 0 \\ 0 & 0 & \frac{1}{4} & 0 & \frac{1}{2} & 0 & 0 & \frac{1}{4} & 0 \\ \frac{1}{2} & 0 & 0 & 0 & \frac{1}{2} & 0 & 0 & 0 & 0 \\ 0 & \frac{1}{4} & 0 & \frac{1}{4} & 0 & \frac{1}{4} & \frac{1}{4} & 0 & 0 \\ 0 & 0 & \frac{1}{4} & 0 & \frac{1}{2} & 0 & 0 & \frac{1}{4} & 0 \\ 0 & 0 & 0 & 0 & \frac{1}{2} & 0 & 0 & \frac{1}{2} & 0 \\ 0 & 0 & 0 & 0 & 0 & \frac{1}{4} & \frac{1}{2} & 0 & \frac{1}{4} \\ 0 & 0 & 0 & 0 & 0 & 0 & 0 & 1 & 0 \end{array}\right) \end{array}. \tag{10}$$

Analytical values for update U_{A_LU}, were calculated using (5). The process was then simulated and U_{S_LU} was calculated using (9).

Table I shows the analytical and simulated values obtained. It is assumed that the mobile user has made 20 steps (each step is a movement across a cell), including the initial position. The relative error computed in each case is tabulated in the third row.

From the entries in this table, it can be seen that the relative error is less than 0.25%, which indicates excellent concurrence between the analytically obtained values and the simulated values.

B. Location-Update Rates in the Hexagon-Cell Model

There are a total of 15 computational states in the hexagon model, out of which 11 are normal states and four are asterisk states for LA size $n = 4$. Table II tabulates the analytical and simulated values obtained using (5) and (9), after the mobile user has moved 20 steps (including initial position). The relative error is also tabulated and can be noticed to be less than 0.9%.

C. Dwell Time

For dwell-time calculations, the regular transition matrix P given in Section III is modified and reproduced below for an absorbing Markov chain. $\mathbf{A}$ is the absorbing state.

$$\mathbf{P} = [p_{ij}] = \begin{array}{c} \\ \mathbf{A} \\ \mathbf{1} \\ \mathbf{2} \\ \mathbf{3} \\ \vdots \end{array}\!\!\begin{array}{c} \begin{array}{ccccc} \mathbf{A} & \mathbf{1} & \mathbf{2} & \mathbf{3} & \cdots \end{array} \\ \left(\begin{array}{ccccc} \mathbf{p_{AA}} & \mathbf{p_{A2}} & \mathbf{p_{A3}} & \cdots & \cdots \\ \mathbf{p_{1A}} & \mathbf{p_{11}} & \mathbf{p_{12}} & \mathbf{p_{13}} & \cdots \\ \mathbf{p_{2A}} & \mathbf{p_{21}} & \mathbf{p_{22}} & \mathbf{p_{23}} & \cdots \\ \mathbf{p_{3A}} & \mathbf{p_{31}} & \mathbf{p_{32}} & \mathbf{p_{33}} & \cdots \\ \cdots & \cdots & \cdots & \cdots & \cdots \end{array}\right) \end{array}.$$

D. Dwell Time in the Square-Cell Model

The transition matrix $\mathbf{P_a}$ for the absorbing Markov chain for the square-cell model $n = 5$ is given as

$$\mathbf{P} = [p_{ij}] = \begin{array}{c} \\ A \\ 1 \\ 2 \\ 3 \\ 4 \\ 5 \\ 6 \end{array}\!\!\begin{array}{c} \begin{array}{ccccccc} A & 1 & 2 & 3 & 4 & 5 & 6 \end{array} \\ \left(\begin{array}{ccccccc} 1 & 0 & 0 & 0 & 0 & 0 & 0 \\ \frac{1}{2} & \frac{1}{2} & 0 & 0 & 0 & 0 & 0 \\ \frac{1}{2} & \frac{1}{4} & 0 & \frac{1}{4} & \frac{1}{4} & 0 & 0 \\ \frac{1}{4} & 0 & \frac{1}{2} & 0 & 0 & \frac{1}{4} & 0 \\ 0 & 0 & \frac{1}{2} & 0 & 0 & \frac{1}{2} & 0 \\ 0 & 0 & 0 & \frac{1}{4} & \frac{1}{2} & 0 & \frac{1}{4} \\ 0 & 0 & 0 & 0 & 0 & 1 & 0 \end{array}\right) \end{array}. \tag{11}$$

The dwell time was then estimated using simulation. The simulation process for dwell time is similar to the simulation process for location update. The average time to absorption is the sum of the times to absorption divided by the number of experiments M_E and is given as

$$\bar{M}(t) = \frac{1}{M_E}\sum_{x=1}^{M_E} M_i(t)(x) = U_{S\_D}. \tag{12}$$

Table III shows the analytical and simulation values obtained for the dwell time for a 5 ∗ 5 square-cell configuration. The relative error was also calculated and was found to be less than 0.2%, which again validated the analytical approach.

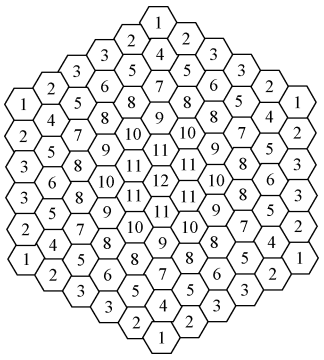

$\mathbf{P_a} =$

	A	1	2	3	4	5	6	7	8	9	10	11	12
A	1	0	0	0	0	0	0	0	0	0	0	0	0
1	1/2	0	1/3	0	1/6	0	0	0	0	0	0	0	0
2	1/3	1/6	0	1/6	1/6	1/6	0	0	0	0	0	0	0
3	1/3	0	1/6	1/6	0	1/6	1/6	0	0	0	0	0	0
4	0	1/6	1/3	0	0	1/3	0	1/6	0	0	0	0	0
5	0	0	1/6	1/6	1/6	0	1/6	1/6	1/6	0	0	0	0
6	0	0	0	1/3	0	1/3	0	0	1/3	0	0	0	0
7	0	0	0	0	1/6	1/3	0	0	1/3	1/6	0	0	0
8	0	0	0	0	0	1/6	1/6	1/6	1/6	1/6	1/6	0	0
9	0	0	0	0	0	0	0	1/6	1/3	0	1/3	1/6	0
10	0	0	0	0	0	0	0	0	1/3	1/3	0	1/3	0
11	0	0	0	0	0	0	0	0	0	1/6	1/3	1/3	1/6
12	0	0	0	0	0	0	0	0	0	0	0	1	0

'A' **means absorbing state**

Fig. 7. Hexagon-cell LA and transition probability for the absorbing Markov chain.

TABLE IV
DWELL TIME IN THE HEXAGON-CELL MODEL (COMPARISON WITH PUBLISHED RESULTS)

S_i	1	2	3	4	5	6	7	8	9	10	11
D_a	6.1423	8.5924	9.5516	13.6633	16.1979	16.968	20.2578	22.2543	25.1793	26.1686	28.1722
D_s	6.142	8.580	9.533	13.627	16.178	16.911	20.224	22.1	25.130	26.104	28.090
RE	0.049	0.145	0.195	0.266	0.123	0.337	0.167	0.246	0.196	0.247	0.293

S_i – Initial state of the user, RE – Relative Error%, D_a – analytically obtained dwell time, D_s- dwell time from published results

E. Dwell Time in the Hexagon-Cell Model

The validation for this part of the analytical model was done with some published results, as they were available. Hence, instead of using the hexagon model of size $n = 4$, which we had used for studying the location-update rates, we now use a hexagon model of size $n = 5$, as published results were available for this configuration in [1]. Fig. 7 shows the numbering of cells and the transition probability matrix for hexagon cell LA with $n = 5$. The asterisk-boundary states of Fig. 5 have been lumped into an absorbing state to derive the dwell time. The $\mathbf{A}$ in the transition matrix indicates the absorbing state and the analytical results obtained from our model are given in Table IV. In addition, in this table we have given the simulated values from [1] for an identical configuration. The relative error tabulated is again within 0.4%. With this, we have provided a second means of validation for the proposed mobility model.

V. HIGHLIGHTS OF THE MODEL

Before we apply the model to the overlapped location-area strategy, we highlight the features of the model that was described.

1) The number of computational states is considerably reduced. Some numerical examples of the state reduction are provided below. We have compared the number of states with a conventional model although work has been done by some researchers [1] to obtain a reduced number of states.

Square-Cell Model

For a normal square-cell LA, the computational states will be $n \times n = n^2$ if a conventional 2-D random-walk model were used. However, in our model, the total states to be considered for computations are significantly reduced to

$$2*\left\lceil n+\frac{1}{2}\right\rceil *+\sum_{n_i=1}^{n}\left\lceil\frac{n_i}{2}\right\rceil. \tag{13}$$

Where both n and n_i are odd

$$2*\left\lceil\frac{n}{2}\right\rceil *+\sum_{n_i=2}^{n-1}\frac{n_i}{2} \tag{14}$$

where both n, n_i are even.

In (13) and (14), the first part alone gives the boundary states; the second part gives the number of states that are not boundary states. Hence, in the equations, the boundary states are multiplied by 2 to take into account the boundary-asterisk states.

To take a typical example, if $n = 5$, the number of computational states in the proposed model would be only nine, whereas in the conventional 2-D model there would be 25.

Hexagon-Cell Model

The total number of states for conventional 2-D random walk model $= 1 + \sum_1^n 6n$. The total number of states in the proposed model is given by

$$\mathrm{n}*+1+\sum_{1}^{n} n \tag{15}$$

where $n*$ are the number of asterisk states.

Taking a numerical example for $n = 4$, the proposed model has 15 states, whereas the conventional model would have 61 states.

2) The regular Markov model so derived can be used for studying location-update rates.
3) A slightly modified model with absorbing states can be used to compute the LA dwell time.

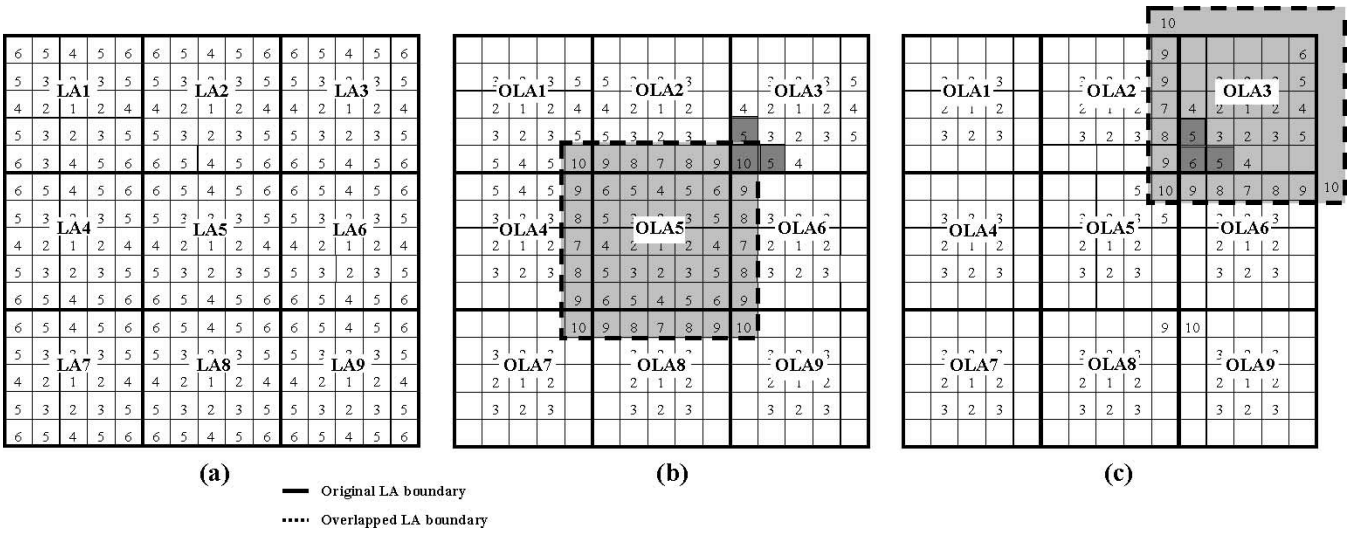

Fig. 8. Cell layout for the OLA strategy.

4) The model can be applied for both square and hexagon cells.
5) The model can be used for static and dynamic location-area strategies.
6) The calculation has been considerably simplified due to the wrap-around technique.

VI. Overlapped Location-Area Modeling

To demonstrate the applicability of the proposed model to study an overlapped location-area strategy, we have chosen the square-cell configuration with size $n = 5$. Most studies use the call-to-mobility Ratio (CMR) to study the location-update rates. The CMR is given by λ_c/λ_m. $1/\lambda_m$ can be defined as the mean residence time for a mobile node in cell and λ_c is the call-arrival rate to the mobile user. In this study, we will estimate the location-update rates versus the inverse of CMR, which we identify as the "movements per call" (MPC). MPC is the number of cell movements or steps that the user makes between call arrivals. This study was conducted for both the nonoverlapped and the overlapped cell configurations. Because of overlap, the LA boundary-crossing rate decreases considerably as the size of the LA has expanded. However, since the total number of LAs is the same as when no overlapping is applied, the average number of mobile users per LA is the same for both overlapped and nonoverlapped approaches.

Fig. 8 shows a comparative picture of a normal LA with 25 square cells and an overlapped LA. Fig. 8(a) shows the normal 25 cells LA with its adjacent LAs. If LA5 is the LA under consideration, then LA2, LA4, LA6, and LA8 are the adjacent LAs, to which the user can move from LA5. Fig. 8(b) shows the overlap between the adjacent LAs. The LAs are now called OLAs (overlapped LAs). The overlapped area of OLA5 is highlighted in Fig. 8(b) and is bounded by the bold broken lines. The corresponding overlap areas of the other LAs can be visualized; the overlap area of LA3 will be OLA3, as shown in Fig. 8(c). The numbers in the cells correspond to the aggregate states identified within an LA earlier, although the numbering order has been changed for convenience of applicability in the overlapped case.

Fig. 8(c) has been provided to help explain the state-transition diagram when the mobile user crosses from one overlapped LA to another; in this case, from OLA5 to OLA3.

In the case of an overlapped LA such as OLA5, there are ten aggregate states, as can be seen in Fig. 8(b). The state-transition diagram for the mobile user movement within and across the boundary of the overlapped LA is given in Fig. 9. Fig. 9(a) shows the transitions within one overlapped LA and Fig. 9(b) shows the transitions from one overlapped LA to another. Similar to the nonoverlapped LA model, asterisk states $2*$, $3*$, and $5*$ [shown in Fig. 9(b)] represent the boundary states of adjacent OLAs.

A brief explanation of the state-transition diagram is given here. Focusing on OLA5 and OLA3 in Fig. 8(b) and (c), we explain the state-transition diagram of Fig. 9. When a user is in state 10 in OLA5, he can transition to state 5 (dark shaded cells) in OLA3 with 1/2 probability. (There are two adjacent states numbered 5 and the transition to each is 1/4.) This is indicated as a transition from state 10 to state $5*$ in Fig. 9(b) with 1/2 probability. The mobile user can also move to state 9 (there are two states numbered 9 that are adjacent to state 10) within LA5 itself with 1/2 probability, which is shown in Fig. 9(a). Once the user has left the overlapped area of OLA5, he is considered to be in the OLA3 coverage area. Hence, if one refers to Fig. 8(c), the OLA3 extended area is explicitly shown. The dark shaded cells in Fig. 8(c) correspond to the dark shaded ones in Fig. 8(b). We notice that the cell numbered 10 in the dark shaded cells of Fig. 8(b) is now numbered 6 in the OLA3 coverage area in Fig. 8(c). From Fig. 8(c), the user in state 5 has a 1/4 probability of moving into state 3, 4, 6, or 8, which is indicated by the transition from $5*$ to states 3, 4, 6, and 8 in Fig. 9(b). This explanation can be extended to understand how the transition diagram was derived. Once the state-transition diagram has been obtained, the transition-probability matrix can be obtained, which is given in the first equation at the bottom of the next page.

From Table I, we get the average number of location updates made by a user making 20 steps. The entries in Table I are tabulated against the starting cell position of the user, i.e., *initial state* S_i. Assuming that there is an equal probability of finding the mobile user in any one of the 25 cells, as his initial position we can obtain the average number of location updates initiated by the user moving within the LA and making $k = 20$ steps using (16) and (17) at the bottom of the page, where LU_n is the average number of updates originating from a *normal* nonoverlapped LA of size n.

The procedure was repeated for different values of k. If no call arrives between the k steps, then (16) gives the average number of updates made by a user roaming in the LA. Hence, k gives the MPC values. We have evaluated the average number of location-update rates for both the overlapped and nonoverlapped cases for various values of MPC and have provided them in Table V.

The MPC carries information similar to CMR, but is its inverse. The MPC shows the number of movements made by the mobile between two calls. For example, if we assume the average MPC is 20, then it means the mobile makes an average of 20 steps or movements across cells between two calls. We have used a range of specific values for MPC for obtaining the average number of location updates initiated by a user roaming within an LA. The entries in the table clearly show that the overlapped LA mechanism has fewer LA update requirements than the normal LA, which is true.

$$\mathbf{P} = [p_{ij}]$$

$$= \begin{array}{c} \\ 2* \\ 3* \\ 5* \\ 1 \\ 2 \\ 3 \\ 4 \\ 5 \\ 6 \\ 7 \\ 8 \\ 9 \\ 10 \end{array} \begin{array}{c} \begin{array}{cccccccccccc} 2* & 3* & 5* & 1 & 2 & 3 & 4 & 5 & 6 & 7 & 8 & 9 & 10 \end{array} \\ \begin{pmatrix} 0 & 0 & 0 & \frac{1}{4} & 0 & \frac{1}{2} & \frac{1}{4} & 0 & 0 & 0 & 0 & 0 & 0 \\ 0 & 0 & 0 & 0 & \frac{1}{2} & 0 & 0 & \frac{1}{2} & 0 & 0 & 0 & 0 & 0 \\ 0 & 0 & 0 & 0 & 0 & \frac{1}{4} & \frac{1}{4} & 0 & \frac{1}{4} & 0 & \frac{1}{4} & 0 & 0 \\ 0 & 0 & 0 & 0 & 1 & 0 & 0 & 0 & 0 & 0 & 0 & 0 & 0 \\ 0 & 0 & 0 & \frac{1}{4} & 0 & \frac{1}{2} & \frac{1}{4} & 0 & 0 & 0 & 0 & 0 & 0 \\ 0 & 0 & 0 & 0 & \frac{1}{2} & 0 & 0 & \frac{1}{2} & 0 & 0 & 0 & 0 & 0 \\ 0 & 0 & 0 & 0 & \frac{1}{4} & 0 & 0 & \frac{1}{2} & 0 & \frac{1}{4} & 0 & 0 & 0 \\ 0 & 0 & 0 & 0 & 0 & \frac{1}{4} & \frac{1}{4} & 0 & \frac{1}{4} & 0 & \frac{1}{4} & 0 & 0 \\ 0 & 0 & 0 & 0 & 0 & 0 & \frac{1}{2} & 0 & 0 & 0 & 0 & \frac{1}{2} & 0 \\ \frac{1}{4} & 0 & 0 & 0 & 0 & 0 & \frac{1}{4} & 0 & 0 & 0 & \frac{1}{2} & 0 & 0 \\ 0 & \frac{1}{4} & 0 & 0 & 0 & 0 & 0 & \frac{1}{4} & 0 & \frac{1}{4} & 0 & \frac{1}{4} & 0 \\ 0 & 0 & \frac{1}{4} & 0 & 0 & 0 & 0 & 0 & \frac{1}{4} & 0 & \frac{1}{4} & 0 & \frac{1}{4} \\ 0 & 0 & \frac{1}{2} & 0 & 0 & 0 & 0 & 0 & 0 & 0 & 0 & \frac{1}{2} & 0 \end{pmatrix} \end{array}.$$

$$\mathrm{LU}_n = \sum_{N=1}^{6} \text{cells in aggregate state } S_N * \frac{U_{A\_\mathrm{LA}}}{(n \times n)} \tag{16}$$

$$\mathbf{P} = [p_{ij}]$$

$$= \begin{array}{c} \\ 2* \\ 3* \\ 5* \\ 1 \\ 2 \\ 3 \\ 4 \\ 5 \\ 6 \\ 7 \\ 8 \\ 9 \\ 10 \end{array} \begin{array}{c} \begin{array}{cccccccccccc} 2* & 3* & 5* & 1 & 2 & 3 & 4 & 5 & 6 & 7 & 8 & 9 & 10 \end{array} \\ \begin{pmatrix} 0 & 0 & 0 & \frac{1}{4} & 0 & \frac{1}{2} & \frac{1}{4} & 0 & 0 & 0 & 0 & 0 & 0 \\ 0 & 0 & 0 & 0 & \frac{1}{2} & 0 & 0 & \frac{1}{2} & 0 & 0 & 0 & 0 & 0 \\ 0 & 0 & 0 & 0 & 0 & \frac{1}{4} & \frac{1}{4} & 0 & \frac{1}{4} & 0 & \frac{1}{4} & 0 & 0 \\ 0 & 0 & 0 & 0 & 1 & 0 & 0 & 0 & 0 & 0 & 0 & 0 & 0 \\ 0 & 0 & 0 & \frac{1}{4} & 0 & \frac{1}{2} & \frac{1}{4} & 0 & 0 & 0 & 0 & 0 & 0 \\ 0 & 0 & 0 & 0 & \frac{1}{2} & 0 & 0 & \frac{1}{2} & 0 & 0 & 0 & 0 & 0 \\ 0 & 0 & 0 & 0 & \frac{1}{4} & 0 & 0 & \frac{1}{2} & 0 & \frac{1}{4} & 0 & 0 & 0 \\ 0 & 0 & 0 & 0 & 0 & \frac{1}{4} & \frac{1}{4} & 0 & \frac{1}{4} & 0 & \frac{1}{4} & 0 & 0 \\ 0 & 0 & 0 & 0 & 0 & 0 & \frac{1}{2} & 0 & 0 & 0 & 0 & \frac{1}{2} & 0 \\ \frac{1}{4} & 0 & 0 & 0 & 0 & 0 & \frac{1}{4} & 0 & 0 & 0 & \frac{1}{2} & 0 & 0 \\ 0 & \frac{1}{4} & 0 & 0 & 0 & 0 & 0 & \frac{1}{4} & 0 & \frac{1}{4} & 0 & \frac{1}{4} & 0 \\ 0 & 0 & \frac{1}{4} & 0 & 0 & 0 & 0 & 0 & \frac{1}{4} & 0 & \frac{1}{4} & 0 & \frac{1}{4} \\ 0 & 0 & \frac{1}{2} & 0 & 0 & 0 & 0 & 0 & 0 & 0 & 0 & \frac{1}{2} & 0 \end{pmatrix} \end{array} \tag{17}$$

TABLE V
LOCATION UPDATE VERSUS MPC (OVERLAPPED AND NONOVERLAPPED CASES)

MPC	1	2	3	4	5	6	7	8	9	10
overlapped	0.138	0.156	0.192	0.228	0.274	0.330	0.392	0.454	0.516	0.577
Non-overlapped	0.192	0.32	0.448	0.608	0.8	1.0	1.2	1.4	1.6	1.8

MPC	11	12	13	14	15	16	17	18	19	20
overlapped	0.639	0.701	0.763	0.825	0.887	0.949	1.010	1.134	1.134	1.196
Non-overlapped	2.0	2.2	2.4	2.6	2.8	3.0	3.2	3.4	3.6	3.8

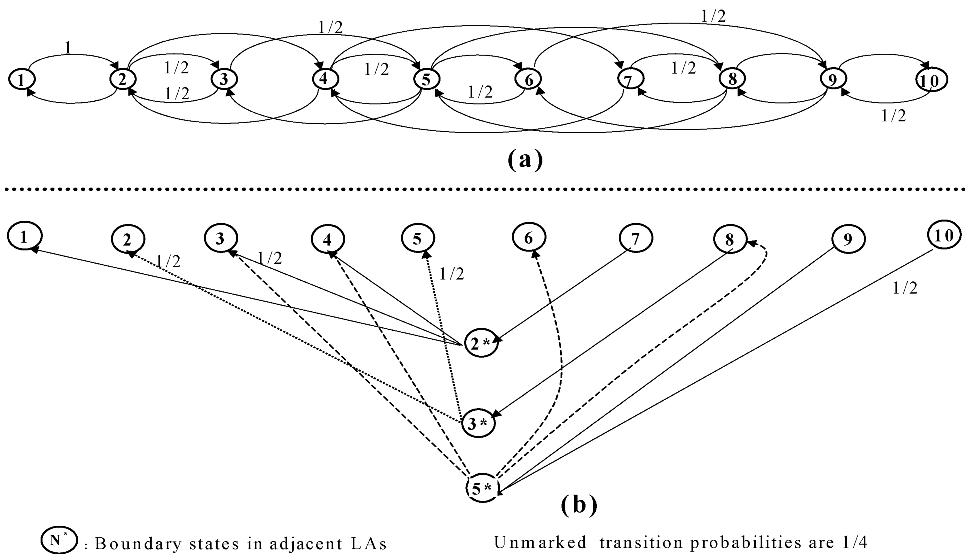

Fig. 9. State-transition diagram for overlapped LA.

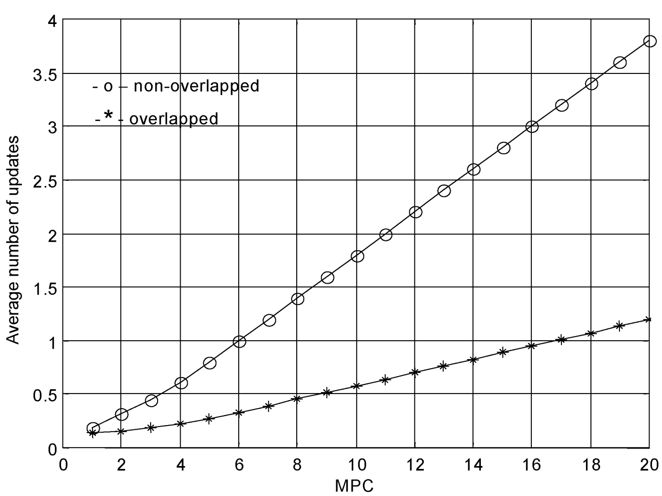

Fig. 10. LA updates and overlapped LA updates versus MPC.

Fig. 10 is plot of the location updates calculated for the normal and overlapped LA cases. From the graph, we notice that the greater the number of movements a user makes between call arrivals (which signifies that he is a fast-moving user), the average number of updates increases with increasing MPC. However, for the overlapped LA case, the number of location updates is considerably less, especially at higher MPC values, which is logically reasonable.

VII. CONCLUSION

Applying 2-D random-walk models to study user mobility in terms of location updates and dwell time in wireless networks has been difficult due to the number of computational states, which one encounters in analytical models. In this work, we have applied the property of "lumped process" to the regular Markov chain and obtained a model with reduced computational states. The model could be used to study location-update rates and dwell time both for the square- and hexagon-cell configurations. The analytical results obtained for location-update and dwell time for the two configurations (square and hexagon) show excellent agreement with the simulation results with relative error less than 1%. The model was further validated with published results. The adaptability of the model has been demonstrated by applying it to a square-cell overlapped LA case.

REFERENCES

[1] I. F. Akyildiz, Y.-B. Lin, W.-R. Lai, and R.-J. Chen, "A new random walk model for PCS networks," *IEEE J. Select. Areas Commun.*, vol. 18, pp. 1254–1259, July 2000.
[2] K. S. Meier-Hellstern and E. Alonso, "The use of SS7 and GSM to support high density personal communications," in *Proc. IEEE ICC'92*, Chicago, IL, June 1992, pp. 1072–1698.
[3] S. Mohan and R. Jain, "Two user location strategies for personal communications services," *IEEE Pers. Commun.*, vol. 1, no. 1, pp. 42–50, 1994.

[4] G. P. Pollini and D. J. Goodman, "Signalling system performance evaluation for personal communications," *IEEE Trans. Veh. Technol.*, vol. 45, pp. 131–138, Feb. 1996.
[5] B. Jabbari, Y. Zhou, and F. Hellier, "Random walk modeling of mobility in wireless networks," in *Proc. IEEE VTC'98*, May 1998, pp. 639–643.
[6] T. X. Brown and S. Mohan, "Mobility management for personal communications systems," *IEEE Trans. Veh. Technol.*, vol. 46, pp. 269–278, May 1997.
[7] I. F. Akyildiz, J. S. M. Ho, and Y.-B. Lin, "Movement-based location update and selective paging for PCS networks," *IEEE/ACM Trans. Networking*, vol. 4, pp. 629–638, Aug. 1996.
[8] D. Lam, D. C. Cox, and J. Widom, "Teletraffic modeling for personal communications systems," *IEEE Commun. Mag.*, vol. 35, pp. 79–87, Feb. 1997.
[9] K.-H. Chiang and N. Shenoy, "Architecture and schemes for intelligent mobility management in future mobile telecommunication systems," in *Proc. IEEE GLOBECOM'00*, San Francisco, CA, Nov. 2000, pp. 1463–1467.
[10] J. G. Kemeny and J. L. Snell, *Finite Markov Chains*. New York: Springer-Verlag, 1976.
[11] T. Tugcu and C. Ersoy, "Application of realistic mobility model in metropolitan cellular systems," in *Proc. VTC'01*, Rhodes, Greece, May 2001, pp. 1047–1051.
[12] W. Su, S.-J. Lee, and M. Gerla, "Mobility prediction in wireless networks," in *Proc. IEEE MILCOM 2000*, Los Angeles, CA, Oct. 2000, pp. 491–495.
[13] J. G. Markoulidakis, G. L. Lyberopoulos, D. F. Tsirkas, and E. D. Sykas, "Mobility modeling in third generation mobile telecommunications systems," *IEEE Pers. Commun.*, vol. 4, pp. 41–56, Aug. 1997.
[14] K. K. Leung, W. A. Massey, and W. Whitt, "Traffic models for wireless communications networks," *IEEE J. Select. Areas Commun.*, vol. 12, pp. 1353–1364, Oct. 2000.
[15] K.-H. Chiang and N. Shenoy, "A random walk mobility model for location management in wireless networks," in *Proc. PIMRC 2001*, vol. 2, San Diego, CA, pp. E43–E48.
[16] M. Mouly and M. B. Pautet. (1992) The GSM system for mobile communication. *Cells Syst.* [Online]. Available: http://citeseer.nj.nec.com/context/39358/0
[17] EIA/TIA, "Cellular Radio-Telecommunications Intersystem Operations,", Washington, DC, Tech. Rep. IS-41, Revision C, 1995.

Kuo-Hsing Chiang received the Diploma from St. John's and St. Mary's Institute of Technology, Taipei, Taiwan, in 1989, the B.E. degree (Hons.) from the Royal Melbourne Institute of Technology (RMIT), Melbourne, Australia, in 1993, and the M.E. degree from Victoria University of Technology, Melbourne, in 1994, all in electrical engineering. He is currently working toward the Ph.D. degree at RMIT.

His research interests are in the area of second- and third-generation mobile communication networks, mobile network architectures, mobility management, and signaling protocols.

Nirmala Shenoy (A'96) received the Ph.D. degree in computer science from the University of Bremen, Bremen, Germany, in 1991 and the B.Eng. degree in electronics and telecommunications engineering and the M.Eng. degree in applied electronics from Madras University, Madras, India, in 1978 and 1980, respectively.

She was a Research Scientist with the Council of Scientific and Industrial Research Laboratories, New Delhi, India. She subsequently took up teaching and has been an Academic in Singapore and Australian universities. She is currently an Associate Professor in the Information Technology Department, Rochester Institute of Technology, Rochester, NY. Her research interests are in the area of Internet quality of service, wireless networks and protocols, mobility models, and management for wireless networks and wireless Internet.